# THE MECHANISM RESEARCH OF DOUBLE STRIKE POINTS OF THE DIVERTOR PARTICLE FLUX IN HL-2A ECRH PLASMAS

N. Wu, L.W. Yan, Z.H. Huang, H.L. Du, W.C. Wang, X.G. Miao, J.M. Gao, J.Q. Xu, Z.B. Shi, Y. Liu, Q.W. Yang, J.Q. Dong, M. Xu and HL-2A Team
Southwestern Institute of Physics
Chengdu, People's Republic of China
Email: wuna@swip.ac.cn

J. Cheng
Institute of Fusion Science, School of Physical Science and Technology, Southwest Jiaotong University
Chengdu, People's Republic of China

## Abstract

Double strike points (DSP) of the particle flux have been observed on the outer divertor target during the HL-2A electron cyclotron resonance heating (ECRH) plasma discharge in the normal magnetic field direction using the Langmuir probe arrays. The analysis shows that the poloidal $E \times B$ drift velocity, which is estimated to be the same order as the ion-acoustic velocity, plays an important role in the forming of the dip of the particle flux. The peak of the electron temperature is far away from the peak of the particle flux in the SOL due to the large radiation of the long leg of the divertor, resulting in an outer shift of the plasma potential peak compared with the particle flux peak, and a positive radial electric field is generated, which is large enough to cause a reversed poloidal $E \times B$ drift flow in the normal magnetic field scenario. What is more, the statistical results show that the DSP phenomenon occurs in the high ECRH power and the low density region, which supports the generation mechanism of the poloidal $E \times B$ drift. The paper highlights the important role of the poloidal $E \times B$ drift and the long leg divertor in the control of the particle flux, which provides some reference for the heat flux mitigation in the future fusion devices.

## 1. INTRODUCTION

A great challenge on the way to commercial fusion is to confine a burning plasma while maintaining tolerable steady state heat and particle flux on the plasma-facing components (PFC). In tokamak plasmas, the power crossing the separatrix enters the scrape-off layer (SOL) characterized with open magnetic field lines, is partly lost via radiation, and most of the power reaches the divertor target. The power in the SOL is usually presented with the exponential decay. The decay length in ITER is estimated to be $\lambda_q \approx 5$ mm [1,2], and the wetted area on the divertor target is small so that the heat load exceeds the material limits 10-15 MW/m$^2$ [3,4]. Therefore, it is an urgent issue to mitigate the heat flux on the divertor target.

One effective way is to increase the depositional area on the divertor target by splitting the strike point. The previous experimental results show that the change of magnetic topology induced by resonant magnetic perturbation (RMP) [5-11] and lower hybrid current drive (LHCD) [12-14] is responsible for the strike point splitting. However, the results in JET-Mark I show non-exponential profiles of particle flux on the outer divertor target in the unfavorable magnetic field direction ($\mathbf{B} \times \nabla \mathbf{B}$ away from the X-point), and an additional peak appears in the private flux region (PFR) when the density increases. This phenomenon occurs in high recycling mechanism, and it disappeared when going to the detachment plasmas[15,16]. The simulation pointed out that the radial $E \times B$ drift can be a candidate for interpreting such phenomenon[17,18]. What is more, the recent study in DIII-D highlights the important role of the poloidal $E \times B$ drift. The double peaking density profiles on the divertor target are attributed to be the significant radial electric field near the divertor target, which leads to a reversed poloidal flow [19]. However, the difference from the result on the JET Mark I is that the double peaks occur in the low recycling plasmas on DIII-D. Both the experiment results on JET Mark I and DIII-D show a dependence of the double peaks of the particle flux on the direction of the toroidal magnetic, i.e. the double peaks occur on the inner divertor but outer divertor target in the normal magnetic field direction.

This work presents the double strike points (DSP) of the divertor particle flux observed by using the divertor Langmuir probe arrays [20] in the HL-2A electron cyclotron resonance heating (ECRH) plasmas, which shows an opposite dependence on toroidal magnetic field compared with the observations on DIII-D and JET Mark I, and it also could not be attributed to change of the magnetic topology as discussed in the previous reports. Therefore, it is necessary to investigate other underlying factors that cause the different observations on HL-2A, which could provide some reference of heat flux control in the future devices. This paper is organized as follows: The experiment setup is presented in section 2; The experiment results with the physical analysis are displayed in the section 3; Finally, the section 4 provides a summary and discussion.

## 2. EXPERIMENTAL SETUP

The HL-2A tokamak has a closed divertor structure with major radius $R = 1.65$ m and minor radius $a = 0.4$ m. Fig. 1(a) shows the cross section. The toroidal arrangements of the Langmuir probe array and the ECRH is displayed in Fig. 1(b). The zoom in views of the divertor structure and the vertical distribution of the Langmuir probe arrays are presented in the Fig.1(c), which shows that the throat is only about 2 cm, and the divertor leg (from the X-point to the divetor target) is relative long, which suggests a long connection length between the upper plasmas and the divertor target near the separatrix. The experiment in this work is carried out with the following discharge parameters: the plasma current is $I_p = 150 - 160$ kA in the anti-clockwise direction, and the central chord-average electron density is $n_e = (0.8 - 2.5) \times 10^{19}$ m$^{-3}$; the electron cyclotron resonance heating (ECRH) with the power of 200 -1400 kW was applied. It is operated in the low single-null (LSN) configuration with toroidal magnetic field $B_t = 1.2 - 1.4$ T in the clockwise direction, i.e. it is the normal $B_t$ with $B \times \nabla B$ pointing to X-point. Four sets of Langmuir probe arrays with 274 tips were installed at two toroidal locations $170^\circ$ apart at inner and outer divertor target plates as shown in the Fig. 1(b). There are 63+63 tips on the inner and outer divertor targets at the position 1, and 74+74 tips on the inner and outer divertor targets at the position 2. The vertical arrangement of the probe arrays with spatial resolution of 6 mm are distributed in the region of $Z = -0.745 \sim -0.865$ m and $Z = -0.755 \sim -0.875$ m on the inner and outer divertor targets, where the negative sign means under the mid-plane, as shown in the Fig. 1(c), which could provide the whole particle flux and temperature profiles around the strike point. The diameter of the probe tip is about 5 mm, and the incident angle between the magnetic line and the divertor target is $\theta \approx 3.5^\circ$, thus the effective receiving area of the probe tip is estimated to be $A_{eff} \approx 1.2$ mm$^2$. The particle flux is calculated according to the expression $\Gamma = I_{sat}/(eA_{eff})$, where $I_{sat}$ is the saturation ion current; the electron temperature is estimated as: $T_e = (V_+ - V_f)/\ln 2$, where $V_+$ and $V_f$ are the positive biased potential and the floating potential, respectively. The data acquisition frequency is 1 MHz.

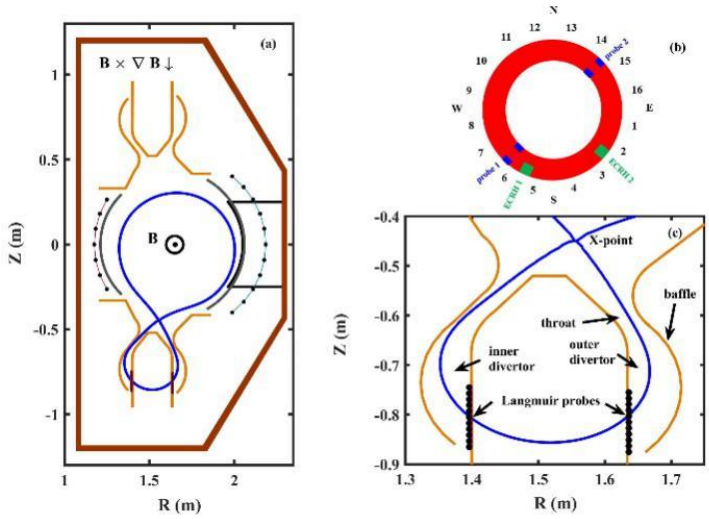


*FIG. 1 (a) The cross section of HL-2A tokamak, (b) the toroidal arrangements of the Langmuir probe arrays and the ECRH, (c) the zoom in view of divertor structure and Langmuir probe arrays.*

## 3. EXPERIMENTAL RESULTS AND ANALYSE

The Fig. 2 shows the forming process of the DSP of divertor particle flux during the ECRH plasma discharge. The electron density normalized with Green density limit $n_G = I_p/\pi a^2$ is displayed in Fig. 2(a). The ECRH with the power of about 610 kW is shown in Fig. 2(b). The spatiotemporal distributions of saturation ion current density on the outer and inner divertor target are provided in Fig. 2(c)-2(d), respectively. Fig. 2(e) shows the distribution of the electron temperature on the outer divertor target. The central chord-averaged electron density and the divertor electron density are compared in Fig. 2(f). The results show that the saturation ion current density and the temperature increase clearly when the ECRH is turned on. In order to investigate the evolution process of the particle flux, four time-windows are highlighted using shadow region with different colours labelled by the capital letters (A, B, C, D). Before the ECRH, the saturation ion current density is relative low and has a single strike point (SSP), as shown by the time-window A; when the ECRH is turn on, it shows an obvious DSP accompanied by an increment of the saturation ion current density (time-window B), and the phenomenon is weakened due to the increment of the normalized electron density. The DSP disappears

completely with the further ramp up of the density, meanwhile, its distribution becomes narrower and the amplitude of the particle flux is enhanced further. However, there is no DSP on the inner divertor target, which is opposite to the phenomenon on DIII-D, in which the DSP occurs on the inner divertor in the normal magnetic field case [19]. It is interesting to observe that the electron temperature on the outer divertor target shows a significant difference during the time-window B when the DSP occurs, and its amplitude is much larger than other time windows. What is more, the DSP is weakened and then disappears with the decrease of the electron temperature on the outer divertor target, which suggests that the temperature is related with the generation of the DSP closely, and further analysis is provided later. There is no DSP in the temperature distribution, which suggests the generation of the DSP could not be attributed to the change of the magnetic topology. The Fig. 2(f) shows that there is an approximate linear relationship between the central chord-averaged density and the divertor electron density, which suggests that the discharge is operated in the sheath-limited regime.

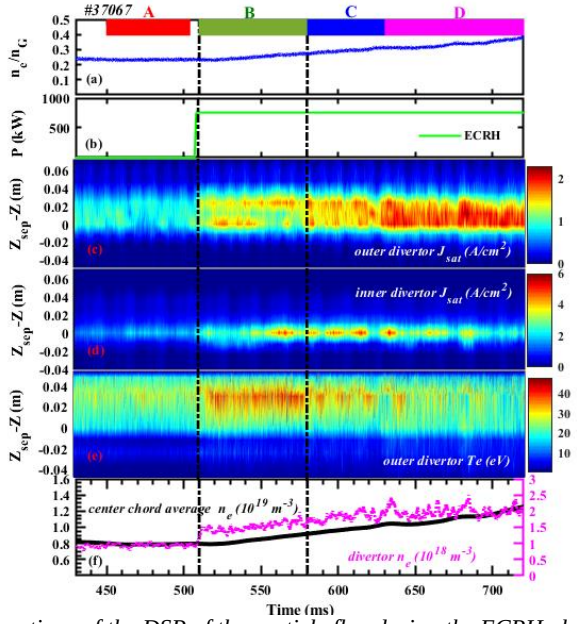


*FIG. 2 The typical experiment observations of the DSP of the particle flux during the ECRH plasmas: (a) the normalized electron density; (b) ECRH power; the distributions of saturation ion current density on the outer (c) and inner (d) divertor target; (e) the electron temperature distribution on the outer divertor target; (f) the central chord-averaged electron density (left Y-axis) and the divertor electron density (right Y-axis).*

In order to investigate the generation mechanism of the DSP, the profiles of the main parameters on the outer diveror target have been presented in Fig. 3. Fig. 3(a) and Fig. 3(b) are the particle flux and electron temperature profiles, respectively. The radial electric field is calculated with the plasma potential estimated by $2.8kT_e + V_f$ [21], as shown in Fig. 3(c), where the positive means the electric field direction to be from the downward to the upward along the vertical target. The poloidal velocity estimated according to $E_r/B_t$ is displayed in Fig. 3(d), and the positive means deviating from the divertor target. The red dashed curves, green solid curves, blue dotted-dashed curves and the purple dotted curves in Fig. 3(a)-(d) represent the average values of the four time-window labelled with A, B, C and D, respectively. As described in Fig. 3(a), the green solid curve shows an obvious DSP, meanwhile the temperature peak as displayed in Fig. 3(b) reaches the maximum as well in this period. The plasma potential is mainly influenced by the electron temperature according to the expression $2.8kT_e + V_f$, thus large temperature gradient indicates large radial electric field and large poloidal electric drift velocity as shown in Fig. 3(c) and Fig. 3(d), respectively. It is important to notice that the temperature peak in the SOL is far away from the strike point, and the dip of the particle flux is located in the positive temperature gradient direction, which results in the poloidal electric drift velocity deviating from the divertor target in the normal toroidal magnetic field case. According to the modified Bohm-Chrodura boundary condition at the entrance of the magnetic presheath [22]: $(B_\theta/B)v_{\|i} + E_r/B = (B_\theta/B)C_s$, the radial drift velocity can influence the particle flux to the divertor target. Assuming the electron temperature $T_e$ is equal to the ion temperature $T_i$, the maximum ion acoustic velocity can be estimated to be $C_s = \sqrt{(T_e + \gamma T_i)/m_i} \approx 50\ \mathrm{km/s}$ based on the temperature shown in Fig. 3(b), where $\gamma$ is the transition factor of the sheath layer and $m_i$ is the ion mass [21]. The poloidal projection of the ion acoustic velocity is about 5 km/s assuming $B_\theta/B \approx 0.1$. The radial electric field is about 1.84 kV/m near the dip of the particle flux, and the poloidal drift velocity is $V_\theta = E_r/B_t \approx 1.44\ \mathrm{km/s}$, which is the same order as the poloidal projection of the ion acoustic

velocity, and it is large enough to influence the total particle flux to the divertor target. In addition, the electron temperature, radial electric field and the poloidal drift velocity decrease with the density increases, therefore, the dip is weakened as shown by the blue curves, and the primary and the secondary peaks are equally matched as shown in Fig. 3(a). The profile of the particle flux becomes more peaking and the peak shows a shift to the PFR region with the density increasing further during the time-window D.

One point should be highlighted is that the leg of the divertor is relative long, which results in large radiation when the energy is transferred to the divertor target along the magnetic field near the separatrix, leading to the outer shift of the temperature peak, which brings two influences on the particle and heat flux: One results in the poloidal drift flow deviating from the outer divertor target in the normal toroidal magnetic field case, which explains the different observations in DIII-D [19]; on the other hand, the peak of the temperature staggers largely that of the particle flux is beneficial to the mitigation of the heat flux on the divertor target, which indicates the advantage of the long leg divertor for the heat flux control.

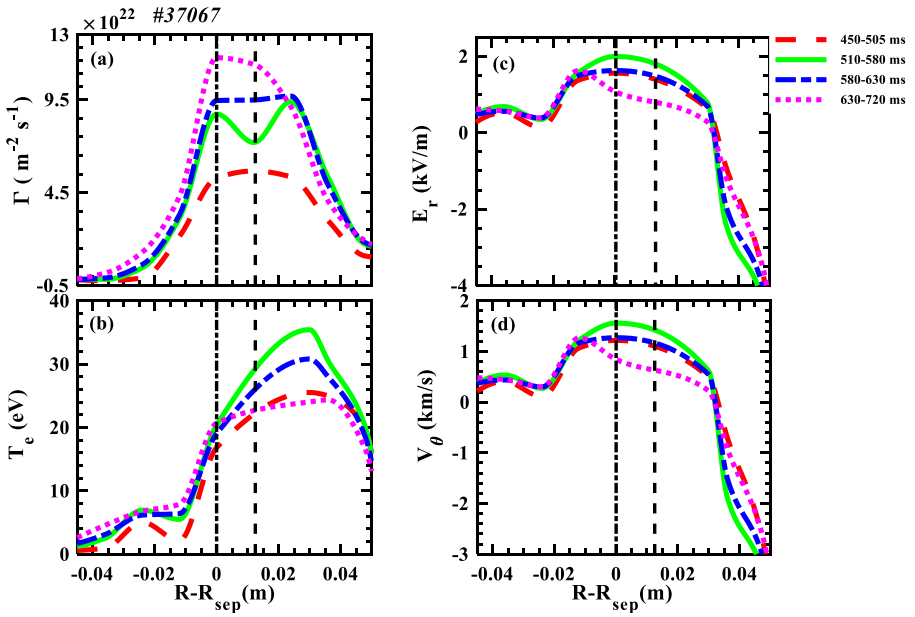


*FIG. 3 The profiles of (a) saturation ion current density, (b) electron temperature, (c) the radial electric field, (d) poloidal velocity on the outer divertor target.*

The secondary peak of the particle flux is formed in the SOL with the density increasing when the ECRH is added in shot 37067, but it appears in the PFR if the electron density decreases with the ECRH as shown by another similar discharge of 34901 in Fig. 4. Fig. 4(a) is the normalized electron density, and the ECRH power is displayed in the Fig. 4(b). The saturation ion current densities on the outer and inner divertor target are shown in the Fig. 4(c) and Fig. 4(d), respectively. Three time-windows with shadows labelled with A, B and C are chosen to distinguish the evolution process of the particle flux, which represent before, during and after the forming of the DSP, respectively. The profiles of the particle flux, which are obtained by taking the average values during the corresponding time-windows, are shown in Fig. 4(c1). The $D_\alpha$ (left Y-axis) and the fueling signals (right Y-axis) are displayed in Fig. 4(e). The results show that the ECRH initiates the DSP of the particle flux on the outer divertor, but the secondary peak appears in the PFR region, which are different from the results in shot 37067. Besides, the formation of the secondary peak lasts about 4 ms as shown by the time-window B. The results suggest that the generation of the DSP could be involved other factor besides of the poloidal $\mathbf{E} \times \mathbf{B}$ drift. The obvious difference between the shots 37067 and 34901 is the evolution of the electron density during the ECRH, and there is a gradual increase of the density in shot 37067, while it shows a decrease in shot 34901. The different evolutions of the density may result in a change of the parallel electron pressure and poloidal electric field direction similar to the results in the paper [17], leading to an opposite radial $\mathbf{E} \times \mathbf{B}$ drift, and thus a different behaviours of the particle flux in the shots 37067 and 34901. However, more data are needed to elucidate this physical process, which will be investigated in the future. What is more, the results show that the fuelling pulses, which may influence the electron temperature and density, could weaken the DSP.

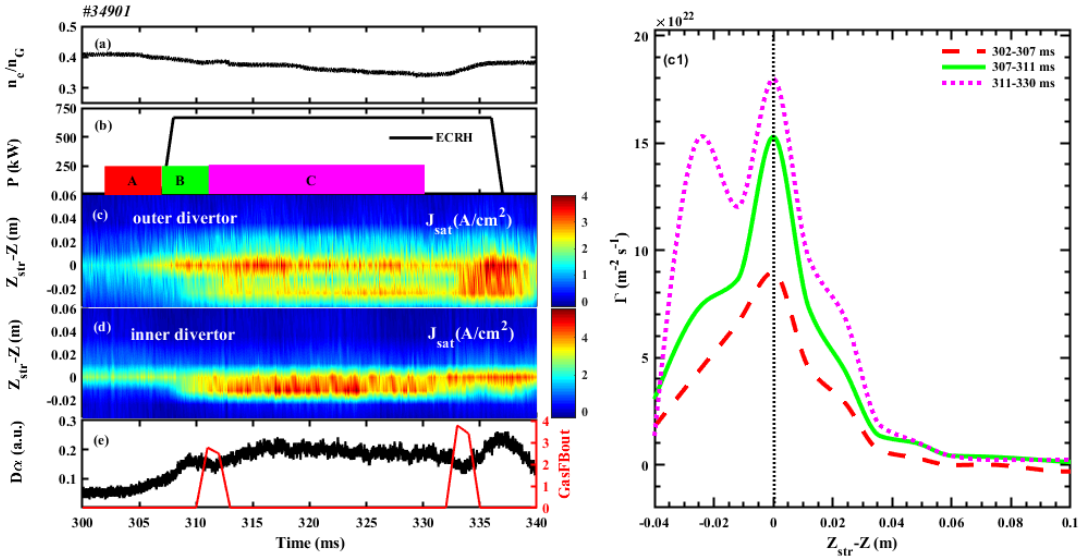


*FIG. 4 (a) The normalized electron density; (b) the ECRH power; the particle flux distribution on the outer (c) and inner (d) divertor target; (e) the $D_\alpha$ (left Y-axis) and fueling signals (right Y-axis) shown by the black and red curves, respectively; (c1) the evolution of the particle flux profiles on the outer divertor target.*

As analyzed above, the DSP of the saturation ion current density shows a closed relationship with the normalized density and the ECRH power, and the corresponding statistical results are presented in the Fig. 5. The horizontal and vertical axises are the normalized electron density and the ECRH power, respectively. The blue squares represent the SSP, and the red circles show the parameter distribution of the DSP. It is clearly shown that the DSP is located at the high ECRH power and lower electron density parameter region, which is consistent with the physics picture on this phenomenon: the electron temperature on the divertor is high with the low density and high ECRH power, which leads to large plasma potential peak, thus a considerable radial electric field is created, which contributes to a reversed particle flux on the outer divertor target in the normal $B_t$ case. However, the radial field generated in the SOL is not large enough to drive the reversed poloidal drift flow for the lower ECRH power and high density case, thus there is only SSP under this condition. What is more, the DSP is usually weaken due to the fuelling pulse, which supports the physical process described above as well.

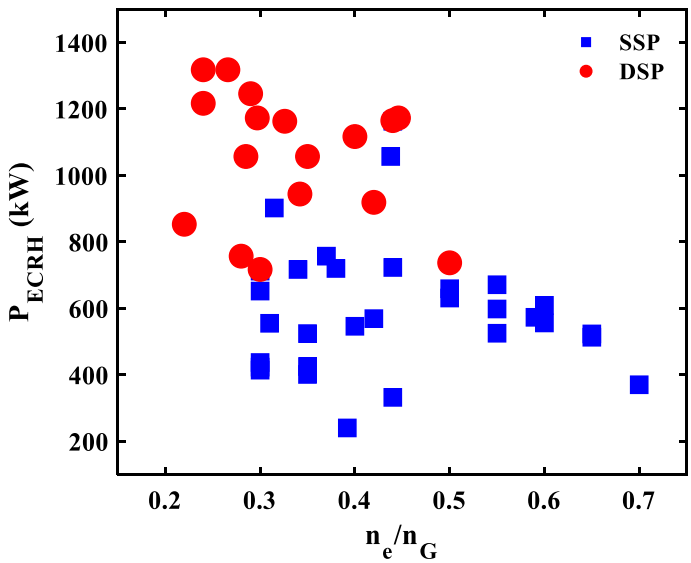


*FIG. 5 The dependence of the DSP on the normalized electron density and the ECRH power*

## 4. SUMMARY AND DISCUSSION

The DSP of the particle flux has been observed on the outer divertor target in the normal $B_t$ case during the HL-2A ECRH plasmas. This phenomenon occurs in the sheath-limited condition. The statistical results show the DSP is located at the lower density and high ECRH power region. The analysis suggests that poloidal $\mathrm{E} \times \mathrm{B}$ drift plays an important role in the generation of the DSP in this scenario. The ECRH leads to large temperature gradient (plasmas potential gradient) in the SOL near the divertor target, and the corresponding poloidal $\mathrm{E} \times \mathrm{B}$ drift velocity is comparable with the ion acoustic velocity according to the calculation based on the Langmuir probe measurement. In addition, the temperature (plasma potential) peak in the SOL is far away from the strike point in the SOL, and the peak of the particle flux is at the positive gradient direction of the temperature (plasma potential), which leads to a reversed poloidal $\mathrm{E} \times \mathrm{B}$ drift flow, thus a dip of the particle flux is formed on the outer divertor target in the normal $B_t$ discharge. The results are different from the observations on DIII-D, where the DSP occurs on the outer divertor target in the unfavourable $B_t$ case [19]. The different behaviours of the particle flux in this work are attributed to the long leg of the divertor on HL-2A, which leads to an outward shift of the temperature peak due to the large radiation near the strike point. This study points out the important role of the poloidal $\mathrm{E} \times \mathrm{B}$ drift in the control of the heat flux and highlights the advantage of the divertor with long leg structure, which provides the reference for the design of the divertor in the future fusion devices.

The DSP may be attributed to different factors in different conditions. The DSP could be observed sometimes in Ohmic discharge when the density is low enough. The error field is easy to penetrate in the low density considering the penetration threshold value $(b_r/B_T)_{crit} \sim n_e B_T^{-1.8} R_0^{-0.25}$ [23], so that DSP in this condition may be attributed to the change of the magnetic topology, and similar phenomenon could be observed in NSTX as well [11]. The error field could not be the main factors that results in the DSP in this work due to the two reasons as follows: (1) The DSP occurs in the process of the density ramp up in shot 37067, which is not beneficial for the penetration of the error field; (2) The DSP on the temperature profile, which could be induced by the change of the magnetic topology due to the error field, is not identified. What is more, the fuelling pulse can weaken the DSP, which supports the physical picture described in this paper as well.

## ACKNOWLEDGEMENTS

This work is supported by National Natural Science Foundation of China under Grant Nos. 11905052, 11875017, 11875020, 11820101004, and National Key R&D Program of China under Grant Nos. 2019YFE03030002, 2019YFE03040002, 2019YFE03090400, 2017YFE0301203, 2017YFE0301106. The authors would like to appreciate the support of Sichuan outstanding youth Science Foundation under Grant No.2020JDJQ0019.

## REFERENCES

[1] Eich T. *et al.* Nuclear Fusion 60, (2020) 056016.
[2] Chang C. S. *et al.* Nuclear Fusion 57, (2017) 116023.
[3] Herrmann A. *et al.* Journal of Nuclear Materials 313-316, (2003) 759-767.
[4] Eich T. *et al.* Nuclear materials and energy 12, (2017) 84-90.
[5] Jia M. *et al.* Plasma Physics and Controlled Fusion 58, (2016).
[6] Thornton A. J. *et al.* Nuclear Fusion 54, (2014) 064011.
[7] Kim K. *et al.* Physics of Plasmas 24, (2017) 052506.
[8] Harting D. *et al.* Nuclear Fusion 52, (2012) 054009.
[9] Muller H. W. *et al.* Journal of Nuclear Materials 438, (2013).
[10] Nardon E. *et al.* Journal of Nuclear Materials 415, (2011) S914-S917.
[11] Ahn J. *et al.* Nuclear Fusion 50, (2010) 045010.
[12] Liang Y. *et al.* Physical Review Letters 110, (2013) 235002.
[13] Xu S. *et al.* Nuclear Fusion 60, (2020) 056006.
[14] Xu S. *et al.* Nuclear Fusion 58, (2018) 106008.
[15] Monk R. D. *et al.* Journal of Nuclear Materials 241-243, (1997) 396-401.
[16] LOARTE A. *et al.* Nucl. Fusion 38, (1998) 331.
[17] Chankin A. V. *et al.* Plasma Phys. Control. Fusion 43, (2001) 299-304
[18] Rognlien T. D. *et al.* Journal of Nuclear Materials 266-269, (1999) 654-659.

[19] Wang H. Q. *et al.* Physical Review Letters 124, (2020) 195002.
[20] Huang Z. H. to be submitted to Journal of Instrumentation, (2021).
[21] Stangeby P. C., The plasma boundary of magnetic fusion devices. (Nicki Dennis, 2000).
[22] Stangeby P. C. *et al.* Physics of Plasmas 2, (1995) 707-715.
[23] Fitzpatrick R. *et al.* Nuclear Fusion 36, (1996) 11-38.